

Symmetry boosts quantum computer performance

Y. S. Nam*

*Department of Computer Science, Institute for Advanced Computer Studies,
and Joint Center for Quantum Information and Computer Science,
University of Maryland, College Park, MD 20910, USA*

R. Blümel

*Department of Physics, Wesleyan University,
Middletown, Connecticut 06459-0155, USA*

(Dated: March 7, 2022)

Abstract

Frequently, subroutines in quantum computers have the structure $\mathcal{F}\mathcal{U}\mathcal{F}^{-1}$, where \mathcal{F} is some unitary transform and \mathcal{U} is performing a quantum computation. In this paper we suggest that if, in analogy to spin echoes, \mathcal{F} and \mathcal{F}^{-1} can be implemented symmetrically such that \mathcal{F} and \mathcal{F}^{-1} have the same hardware errors, a symmetry boost in the fidelity of the combined $\mathcal{F}\mathcal{U}\mathcal{F}^{-1}$ quantum operation results. Running the complete gate-by-gate implemented Shor algorithm, we show that the fidelity boost can be as large as a factor 10. Corroborating and extending our numerical results, we present analytical scaling calculations that show that a symmetry boost persists in the practically interesting case of a large number of qubits. Our analytical calculations predict a minimum boost factor of about 3, valid for all qubit numbers, which includes the boost factor 10 observed in our low-qubit-number simulations. While we find and document this symmetry boost here in the case of Shor's algorithm, we suggest that other quantum algorithms might profit from similar symmetry-based performance boosts whenever $\mathcal{F}\mathcal{U}\mathcal{F}^{-1}$ sub-units of the corresponding quantum algorithm can be identified.

PACS numbers: 03.67.Lx, 03.67.Ac

*Electronic address: ynam@umd.edu

Introduction

The second half of the 20th century saw the advent of the information technology revolution. There is no doubt about its profound impact on just about every aspect of modern society. The technological innovation in computers and networks enabled us to achieve tasks previously thought to be impossible, such as weather forecast, telecommunication, the Global Positioning System, and online banking.

While the current classical technology is already impressive, yet another revolution is about to emerge: Quantum information technology [1]. Taking advantage of quantum superposition and entanglement, a quantum information device is expected to be more secure and faster than its classical counterpart. Epitomizing the latter is Shor's algorithm [1, 2], which enables us to factor a semiprime $N = pq$, where p and q are prime numbers, exponentially faster than any classical algorithm known to date. Shor's algorithm is often associated with code-breaking, since semiprime factorization is at the heart of the widely-employed Rivest-Shamir-Adleman (RSA) encryption algorithm [1, 3].

Despite all the theoretically predicted stupendous powers of quantum information devices, we do encounter major challenges when it comes to a physical realization of these devices: Errors and defects. This is so, because quantum information processors are known to be susceptible to the detrimental effects of inexact gate operations and decoherence, especially for a quantum computer whose workings are based on exquisite control of quantum superposition and interference. An early list of the potentially dangerous physical mechanisms that may destroy the proper functioning of a quantum computer was compiled by Landauer [4], and much progress has been made to fight these adverse mechanisms over the past couple of decades. For instance, overcoming the stochastic type of errors, i.e., errors that occur on a single qubit probabilistically, was the invention of quantum error correction [5–8] and its fault-tolerant implementation [9–11], culminating in the standard de facto approaches of topological and surface codes (see [12] and references therein).

Still, if we are to truly realize a working, physical quantum computer that is practically useful, the limits of engineering must be taken into consideration. Otherwise, a quantum computer will remain an academically interesting device of no practical relevance. One way to approach this problem is to investigate the accuracy gain in logical operations on a logical qubit, given the technology-dependent physical qubit error rate. Pioneering work

in [13], for instance, is already making headway in this direction. Yet, another way to help realize the full potential of quantum computing is to investigate the algorithmic performance behavior at the logical qubit level, providing quantum experimentalists and engineers with a logical error-rate target, potentially easing the physical accuracy and precision requirements. Adding to recent experimental breakthroughs, such as reported in [14] and [15], this paper provides a powerful additional strategy for realizing a working, physical quantum computer.

Methods

As a testbed algorithm we chose Shor’s algorithm, implemented according to Beauregard’s architecture [16]. We selected this particular architecture based on the facts that (i) Shor’s algorithm is arguably the most interesting and most important quantum algorithm to date, (ii) the algorithm is complex enough to realistically capture the effects of faulty gates, and, most importantly, and exploited in this paper, (iii) Beauregard’s architecture allows us to take advantage of symmetry. Whether some other Shor algorithm architectures, such as those presented in [17] (and references therein), may be exploited in a similar fashion is currently under investigation and the results will be reported elsewhere.

Studies addressing the effects of errors and defects on a quantum computer running Shor’s algorithm continue to be of central interest to many scientists. A list of early, notable contributions includes the investigations by Cirac and Zoller [18] studying the effect of errors in interaction time and laser detuning, Miquel *et al.* studying the effects of interactions with a dissipative environment [19] and phase drift errors [20], Wei *et al.* exploring the effects of coherence errors occurring while the quantum computer is idling [21], and García-Mata *et al.* simulating static imperfections in Shor’s algorithm [22]. Recent developments in quantum simulation software [23, 24] reflect the fact that quantum computers remain at the forefront of research. Our work extends this line of research in that we simulate the entire Shor algorithm, gate-by-gate. Based on this complete implementation of Shor’s algorithm, we investigate the effects of errors in the phase-rotation gates.

We note that our error model, to be discussed in the following, reflects the effects of hardware errors that are unavoidable and guaranteed to occur in any hardware that exists in nature. This is so, because even in principle there exists no physical equipment that will meet the mathematically exact circuit specifications. As a consequence, even if the quan-

tum computer is protected with hardware implementing quantum error correction circuitry according to any quantum error correction protocol, each and every single physical quantum gate of the protection circuit will inevitably contain hardware errors. Thus, because hardware errors affect all qubits, including the qubits of the correction circuitry, there is no type of hardware error that would be correctable. In fact, it can be shown (see Supplementary Material) that hardware errors, omnipresent everywhere in a quantum computer, may be more significant than the commonly-addressed locally stochastic errors, often thought to be the most significant source of instability of quantum computers. Our error model, therefore, includes the effects of physical errors, i.e. hardware errors, that are of prime importance for stable quantum computation and, as shown in the Supplementary Material, may indeed be more important than local stochastic errors.

Since the most frequently used quantum gate in Beauregard’s architecture of Shor’s algorithm is a phase rotation gate

$$\theta_j^{(\pm)} = \begin{pmatrix} 1 & 0 \\ 0 & e^{\pm i \frac{\pi}{2^j}} \end{pmatrix}, \quad (1)$$

which appears $\sim 18L^4$ times throughout the algorithm [25] when using the minimally required number of qubits to factor a semiprime N whose bit-length is L , we tested the sensitivity of this quantum computer running Shor’s algorithm with respect to errors in $\theta_j^{(\pm)}$. Specifically, we used a statistical error model of the rotation gate of the form [26]

$$^R\theta_j^{(\pm)} = \begin{pmatrix} 1 & 0 \\ 0 & e^{\pm i \frac{\pi}{2^j} (1 + \alpha^{(\pm)})} \end{pmatrix}, \quad (2)$$

in the case where the errors scale according to the size of the gate operation and

$$^A\theta_j^{(\pm)} = \begin{pmatrix} 1 & 0 \\ 0 & e^{\pm i (\frac{\pi}{2^j} + \alpha^{(\pm)})} \end{pmatrix}, \quad (3)$$

in the case where the errors do not scale according to the size of the operation. In both cases $\alpha^{(\pm)}$ is the defect parameter that may or may not be (strongly) correlated with the gate type indexed with j . In case a one-to-one correlation exists, we call the error “typed” and replace $\alpha^{(\pm)}$ with $\alpha_j^{(\pm)}$. The \pm sign corresponds to forward and backward operation.

The reason why we explicitly distinguish these two error models is as follows. First, any physical device has a finite accuracy, and this is usually given in terms of percentage error

with respect to the size of the gate operation. Since a rotation gate θ_j is built according to a gate decomposition sequence (see references in [27]), the approximated rotation gate will contain errors that scale in the size of the operation, especially regarding the construction method of θ_j , for instance by applying θ_{j+1} twice. This iteration method may be realistic and desirable from the technological or economical perspective. Thus, characterizing a device in terms of relative errors is captured by the $^R\theta_j^{(\pm)}$ model. However, suppose we characterize our quantum computer device in terms of its technological limit, say δ . In this case, most likely, all gates are to be made with different sequences resulting in an error level $\lesssim \delta$, and this is captured by our model $^A\theta_j^{(\pm)}$.

We now subdivide both models into 3 categories: (i) typed errors ($\alpha^\pm = \alpha_j^\pm$), asymmetric ($\alpha^+ \neq \alpha^-$), (ii) typed errors ($\alpha^\pm = \alpha_j^\pm$), symmetric ($\alpha^+ = \alpha^-$), and (iii) non-typed errors, i.e., completely random α^\pm . The three categories are explained as follows. Typing arises from using the same sequence, or the same physical device, for the same θ_j that occur multiple times throughout the entire Shor algorithm. Then, depending on the way that the physical device is set up, since the backward gate is nothing but a unitary inverse of the forward gate, we may assume that the errors of the forward and backward gates are symmetric. Therefore, while (i) and (ii) capture systematic errors, (iii) deals with random errors.

Results

To start with, we simulate the case of factoring $N = 15$. This is the case used in [20], which allows us to compare our results with the results in [20]. Defining the fidelity $F = |\langle \Psi_{\text{actual}} | \Psi_{\text{ideal}} \rangle|^2$ as in [20], in Fig. 1 we plot F as a function of σ , where the errors $\alpha^{(\pm)}$ are Gaussian distributed random variables with mean 0 and standard deviation σ . Consistent with the results presented in [20], the fidelity F of Shor's algorithm follows the form $F = \exp(-\gamma\sigma^2)$ for small σ . At first glance, we observe that the performance of the quantum computer improves in the order of asymmetric, random, and symmetric errors. In particular, symmetric errors give rise to a fidelity boost in $1/\gamma$ by an astonishing factor of ~ 100 in both the $^R\theta_j^{(\pm)}$ and the $^A\theta_j^{(\pm)}$ models. In other words, to obtain comparable F , symmetric errors allow for about a factor 10 larger σ .

The important question to ask now is whether the symmetry-driven fidelity boost will

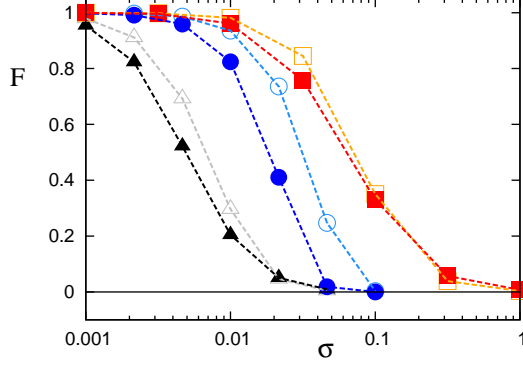


FIG. 1: Fidelity F of a quantum computer factoring $N = 15$ with seed 2 as a function of standard deviation σ of the logical-gate errors. The quantum computer is equipped with adders that are suitable for use in Shor-algorithm factoring of at most 4-bit semiprimes. Shown are the cases of typed, asymmetric errors (triangles), typed, symmetric errors (squares), and non-typed, random errors (circles). Filled plot symbols (red, blue, and black) denote relative errors [see Eq.(2)] and the open plot symbols (orange, cyan, and grey) denote absolute errors [see Eq.(3)]. Dashed lines connecting plot symbols are drawn to guide the eye. The solid, horizontal line corresponds to $F = 0$.

persist as we scale up the quantum circuitry. To start with, we compare the expected fidelities from naively multiplying the fidelities of the basic building blocks of Shor's algorithm, i.e., the quantum adders. This product formula of fidelities has been shown in [20] to work well in the uncorrelated random cases (see also the Supplementary Material).

For an $L + 1$ bit sized quantum adder, capable of executing $s + a$, where s and a are integers of bit length $\leq L$, one may show that the phase Φ associated with $s + a$ in the symmetric case is given by

$$\Phi_{s,a}(l) = \frac{1}{2^{L+1}} \left[1 + \exp \left(i \left\{ \left[\sum_{\nu=0}^{L-1} k_{\nu} r_{L-\nu-1} \right] \right\} \right) e^{2\pi i(s+a-l)/2^{L+1}} \right] R_{s,a}(l), \quad (4)$$

where $k_{\nu} = s_{[\nu]} + a_{[\nu]} - l_{[\nu]}$, where $s_{[\nu]}$, e.g., denotes the ν th binary digit of s ,

$$R_{s,a}(l) = \sum_{l'=0}^{2^L-1} \exp \left[i \left(\sum_{m=0}^{L-1} l'_{[L-1-m]} \left\{ a_{[m]} r_0 + \left[\sum_{\nu=0}^{m-1} k_{\nu} r_{m-\nu} \right] \right\} \right) \right] e^{2\pi i(s+a-l)l'/2^L}, \quad (5)$$

r_j may be α_j or $(\pi/2^j) \times \alpha_j$ if the errors are of an absolute kind or of a relative kind,

respectively, and l is the output integer. The non-typed error cases are obtained by removing correlation via letting each term in k_ν be associated with individual random terms, followed by removing typing of errors associated with the subscript j of r_j .

Calculating now the fidelity of the quantum adder $F_{\text{adder}} = |\Phi_{s,a}(l = s + a)|^2$, using (4) and (5) and assuming that the central limit theorem holds, we find in the limit that L is large and σ is small

$$\begin{aligned} \frac{\min_{s,a} \left| \ln \left(R F_{\text{adder}}^{\text{Typed,Sym}} \right) \right|}{\left\langle \left| \ln \left(R F_{\text{adder}}^{\text{Non-Typed}} \right) \right| \right\rangle_{s,a}} &\approx \frac{1}{3}, & \frac{\max_{s,a} \left| \ln \left(R F_{\text{adder}}^{\text{Typed,Sym}} \right) \right|}{\left\langle \left| \ln \left(R F_{\text{adder}}^{\text{Non-Typed}} \right) \right| \right\rangle_{s,a}} &\approx \frac{11}{18}, \\ \frac{\min_{s,a} \left| \ln \left(A F_{\text{adder}}^{\text{Typed,Sym}} \right) \right|}{\left\langle \left| \ln \left(A F_{\text{adder}}^{\text{Non-Typed}} \right) \right| \right\rangle_{s,a}} &\approx 0, & \frac{\max_{s,a} \left| \ln \left(A F_{\text{adder}}^{\text{Typed,Sym}} \right) \right|}{\left\langle \left| \ln \left(A F_{\text{adder}}^{\text{Non-Typed}} \right) \right| \right\rangle_{s,a}} &\approx 1. \end{aligned} \quad (6)$$

We see from (6) that exploiting symmetry in our circuitry improves the fidelity of the quantum computer. In particular, the symmetry-driven boost always exists, outperforming the average fidelity of the non-typed random cases at all times asymptotically. Based on the naive product formula of fidelities, we conclude that the symmetry-driven fidelity boost persists in large-scale quantum circuits that are of practical interest.

Now, the observed boost in Fig. 1 appears larger than what may be expected from (6), in particular in the case of relative errors. This motivates us to find additional boost mechanisms that are not captured by the naive adder-fidelity product approximation of the Shor processor fidelity. While we were not able to pin down all boost mechanisms, we present in the following the one that is based on the next-level-up building blocks, namely the modulo addition gates.

To start, we point out that a modulo-addition gate consists of five adders and an auxiliary qubit (see, e.g., Fig. 5 of [16]). For an input integer value of s , a quantum modular addition of $s + a \bmod N$ may be performed by first adding a then subtracting N , followed by a conditional operation of adding back N if $s + a < N$, which may be done with the help of an auxiliary qubit. This completes the computational part of the modular addition. In order to now unitarily restore and decouple the auxiliary qubit that is at this point in its conditional state (depending on the relation between $s + a$ and N), two additional adders

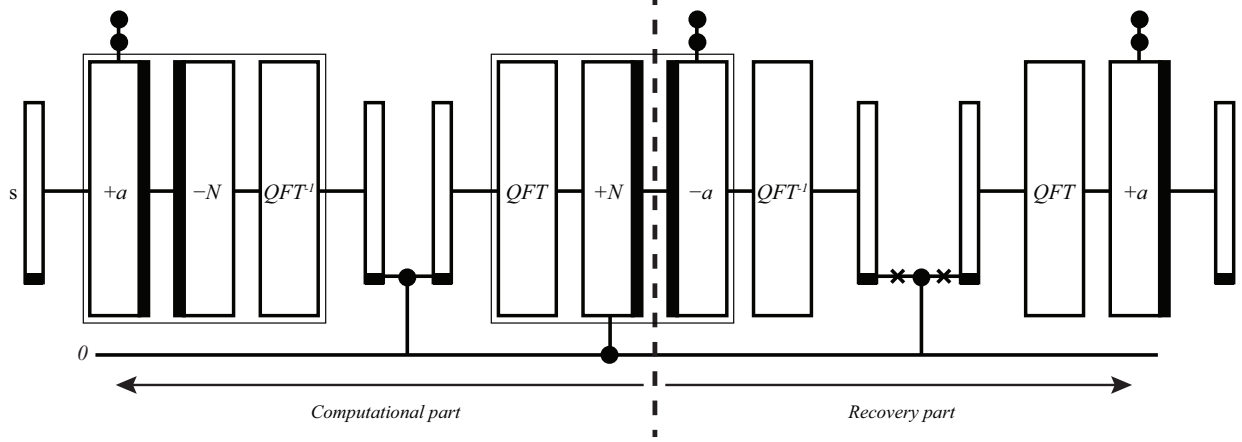


FIG. 2: Modulo addition gate circuit diagram, inspired by Fig. 5 of [16]. Circles denote controlling qubits and Xs denote NOT gates. Thick black bars identify adders and subtractors, i.e., bar-right for adders and bar-left for subtractors. Black solid squares in the qubit register, denoted by thin rectangles, denote the most significant digit qubit of the register. All additions and subtractions are performed in the Fourier space. Solid grey boxes denote the symmetric parts used in the derivation of $F_{s.s.}$ discussed in the text. The dashed line denotes the border between computational and recovery parts of the modulo addition circuit.

that subtract and add a , respectively, are used. We refer to this step as the recovery part of the modular addition.

According to whether the conditional addition of N is triggered or not, we consider two cases, i.e., (i) $s + a < N$ and (ii) $s + a \geq N$. In the former case, because of the triggering, the modulo-addition circuit attains a symmetric substructure, denoted by the solid lines in Fig. 2. Thus, motivated by the existence of the highly organized structure and in the limit of small errors, we write the fidelity of a modulo-addition gate in case (i) as $F^{(i)} \approx F_{s.s.} F_{\text{adder}}^{(a)}$, where $F_{s.s.}$ denotes the fidelity associated with the symmetric substructure and $F_{\text{adder}}^{(a)}$ denotes the fidelity of the last adder with addend a in Fig. 2, all equipped with symmetric noise. In the latter case, the auxiliary qubit is not turned on, resulting in the modulo addition gate fidelity of case (ii) $F^{(ii)} \approx F_{\text{adder}}^{(-N)} F_{\text{adder}}^{(a)}$, assuming that, in the limit of small errors, the errors commute and thus the errors associated with the first adder of the computational part of the modulo addition gate approximately cancel those associated with the first adder (subtractor) of the recovery part of the modulo addition gate.

At this point we notice that the only unknown term is $F_{s.s.}$, since the fidelity of the

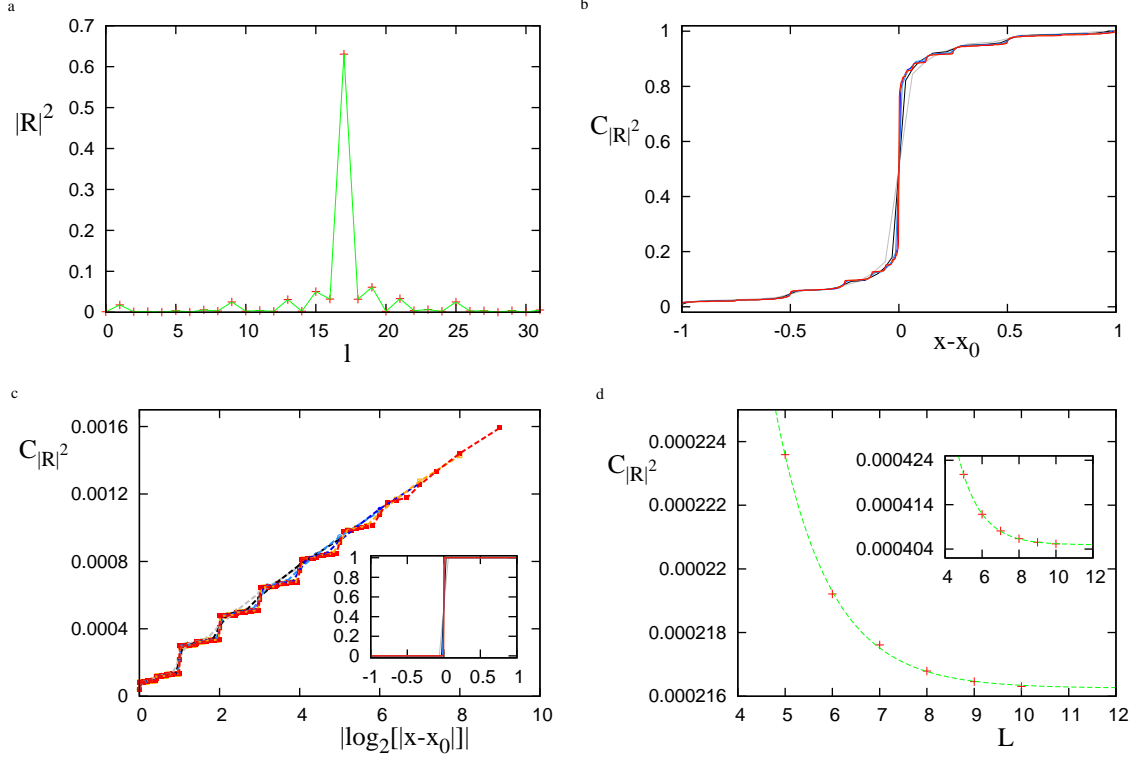


FIG. 3: Various quantities related to R in (5) for relative, symmetric noise for $s = 0$, $a = 0$, and $N = 2^L - 1$. a shows $|R|^2$ as a function of l for $N = 2^4 - 1$, where $\sigma = 0.2$. b shows the corresponding cumulative $|R|^2$, $C_{|R|^2}(x = l/2^{L-1}) = [|R(l)|^2 + |R(l)|^2]/2$, c shows $C_{|R|^2}$ for $\sigma = 0.01$ as a function of $|\log_2[|x - x_0|]|$; inset shows an equivalent plot to b. For both b and c, in the order of grey, black, cyan, blue, orange, and red, $L = 4, 5, \dots, 10$, respectively. d shows an exponential convergence of $C_{|R|^2}$ for $\log_2[|x - x_0|] = 1$ (see inset for $\log_2[|x - x_0|] = 2$) as a function of L .

quantum adder has already been discussed earlier in this paper. Therefore, we now focus on $F_{\text{s.s.}}$.

Defining P_{remain} as the probability of obtaining the ideal bit value of the most significant qubit right after the first box in Fig. 2, one may show $F_{\text{s.s.}} = P_{\text{remain}}^2$. Now, $P_{\text{remain}} = \sum_{l > 2^L} |\Phi_{s,a-N}(l)|^2$, where $\Phi_{s,a-N}$ is nothing but (4) with $a_{[\nu]} \rightarrow a_{[\nu]} - N_{[\nu]}$ and $a \rightarrow a - N$. In fact, we may write $\Phi_{s,a-N}(l)$ as $\cos[\pi(s + a - N - l)/2^L + \sigma^{(\nu)}]|R_{s,a-N}|/2^{L+1}$ up to a phase, where $\sigma^{(\nu)}$ is the sum in the exponent in (4). The remaining term is $|R_{s,a-N}|$, which we analyze next.

In order to gain analytical insight, we consider $s = 0$, $a = 0$, and $l = -N$. In this case,

R has a structure where aligned phasors add up with small phase-angle perturbations of the form $\sum_m -l'_{[L-2-m]} N_{[m]} \pi r_0$. In all other cases ($l \neq -N$), the phasors interfere destructively with the additional perturbation of the ν -sum in (5). Now, because the interference without noise is perfect, the existence of the perturbation gives rise to a non-zero, imperfect interference. Thus, the nature of the imperfection determines $|R|$. We find that [see Fig. 3 a-c for sample cases with $N = 2^L - 1$ and relative errors] whenever the Hamming distance between $-N$ and l is 1 (or small), i.e., $|l - (-N)| = 2^\mu$, where μ is an integer, the magnitude $|R_{l,N}|$ is relatively large (compared to $|l - (-N)| \neq 2^\mu$). This is consistent with our analytical understanding that the more k_ν 's become non-zero, the more randomness is introduced to the perturbation angle, resulting once again in destructive interference, but this time of a statistical nature. In fact, we confirm its manifestation in the modulo addition $0 + 0 \bmod N$ fidelity F for all odd semiprimes $N < 2^{13}$, as shown in Figs. 4 a and b; Semiprimes N between 2^j and 2^{j+1} are sectioned into different F -bands, arising from the bit-spectra of different N values, i.e., the binary digit 1 in the digit spectrum of N turns on the corresponding noisy rotation gate operation.

We also notice that, based on Fig. 2 c, $|R|$ is localized in l . This is expected, since the form of R in (5) remains the same as a function of L while the associated cumulative errors are bounded due to the exponential scaling of the error terms in L . In fact, the sum of $|R|^2$ for $|l - N| < 2^{L-1}$ equals 1 (see Fig. 2 b), where $R(l) = R(l + 2^{L+1})$. We explicitly confirm numerically that the convergence toward the limiting, localized distribution is exponentially better for increasing L (see Fig. 4 d).

Together with the observed localization, we find P_{remain} to be constant as a function of increasing L ($\sigma^{(\nu)}$ is bounded). This is consistent with the plateau behavior observed in Fig. 3 c, in which, to highlight the result shown in Fig. 3 a, we averaged F over N in logarithmic scale, i.e., $2^j < N < 2^{j+1}$ for $j = 3, 4, \dots, 12$, and plot the results (see Fig. 4 d for the average results for Fig. 4 b). In contrast to the relative kind of errors, the case of absolute errors is known to have a fidelity scaling that is one power less favorable in L in the exponent of fidelity (see, e.g., [28]), and this is manifestly visible in Fig. 4 d.

Following the localization result demonstrated in Figs. 3 c and d, assuming the fidelity F_{adder} of a quantum adder predicts the limiting distribution to a very good approximation,

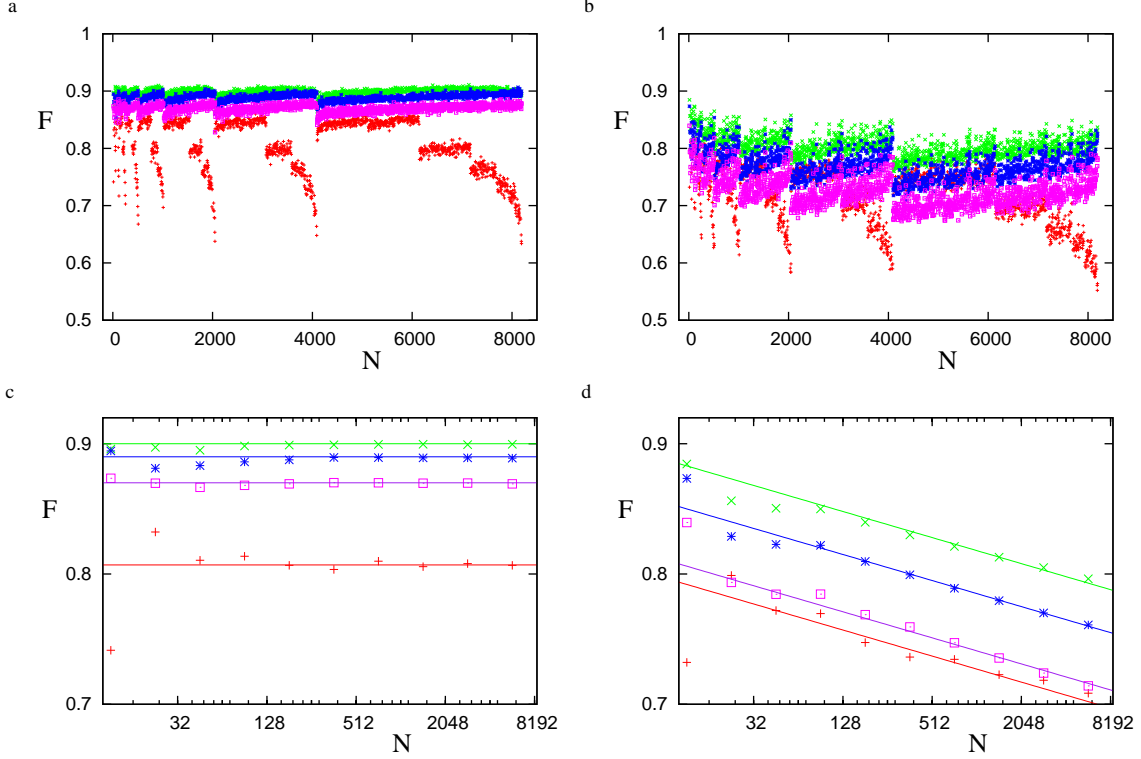


FIG. 4: Fidelity F of a modulo-addition gate performing $0 + 0 \bmod N$, where N is a semiprime. Frames a and b show F as a function of all odd semiprimes $N < 2^{13}$ for relative and absolute symmetric errors, respectively. The error strength used is $\sigma = 0.2$. In the order of pluses (red), crosses (green), asterisks (blue), and squares (purple), the adders are equipped with 0, 1, 2, and 3 additional qubits than minimally required. Frames c and d show logarithmically averaged F , i.e., each point plotted at $2^{j+1/2}$ is the result of averaging over N from 2^j to 2^{j+1} , where $3 \leq j \leq 12$. Notice that for $j = 3$ and $j = 4$, there is only one semiprime each, namely, 15 and 21, respectively, resulting in larger fluctuations due to insufficient statistics. Solid lines in Frame c, with corresponding color symbols, are the tail-region fit lines $F = 0.807, 0.9, 0.89$, and 0.87 . Solid lines in Frame d, with corresponding color symbols, are the tail-region fit lines (to first order) $F = -0.01 \log_2(N) + k$, where $k = 0.827, 0.918, 0.885$, and 0.841 for the four cases shown.

we may write

$$|R(x = l/2^{L-1})|^2 \approx \frac{\eta}{2 \ln(2) |x - x_0|} e^{-\eta[1 + \log_2(1/|x - x_0|)]}, \quad (7)$$

where x_0 is the scaled, ideal output and we used $F_{\text{adder}} = e^{-\eta L}$ from [28], where η is a

constant. Approximating now the sum over $l > 2^{L-1}$ in P_{remain} as an integral, together with $|R(x)|$ in (7), we obtain

$$P_{\text{remain}} \approx \int_0^1 \cos^2 \left[\frac{\pi(x - x_0)}{2} \right] |R(x)|^2 dx, \quad (8)$$

where we assumed $\sigma^{(\nu)}$ is small. This completes our analytical calculation for the only unknown term $F_{\text{s.s.}}$.

Equipped with our analytical fidelity scaling formulae, we once more check for the symmetry-driven fidelity boost. For a sufficiently large quantum circuit, such as Shor's algorithm factoring large semiprimes that are of practical interest, the input s of a modulo addition gate performing $s + a \bmod N$ may range anywhere between 0 and $N - 1$. This results in an approximately 50/50 chance of (i) $s + a < N$ and (ii) $s + a \geq N$, assuming a random s and a uniformly distributed between 0 and $N - 1$. Thus, we expect the average fidelity $F_{\text{add-mod}}$ of a modulo addition gate to be $0.5[F^{(\text{i})} + F^{(\text{ii})}]$. Now, the addition of the addend a of the modulo addition $s + a \bmod N$ occurs with probability $1/4$, assuming random bit values of the two controlling qubits of the addition (see Fig. 5 of [16] for detail). Therefore, assuming once again that the product formula of fidelity holds, this time applied to the modulo addition gate, of which there are $4L^2$ in one complete run of Shor's algorithm, we obtain the symmetric noise Shor fidelity

$$F_{\text{Shor}}^{(\text{Sym})} = F_{\text{add-mod}}^{4L^2} = \left(\frac{3}{4}F_{\text{s.s.}} + \frac{1}{4} \left[\frac{F_{\text{s.s.}}F_{\text{adder}} + F_{\text{adder}}^2}{2} \right] \right)^{4L^2}. \quad (9)$$

This may be compared to

$$F_{\text{Shor}}^{(\text{Non-Typed})} = \left[\frac{3}{4}(F_{\text{adder}})^2 + \frac{1}{4}(F_{\text{adder}})^5 \right]^{4L^2} \quad (10)$$

for the uncorrelated noise counterpart. Importing F_{adder} from Equation (19) of [28], we obtain, for instance, ${}^R F_{\text{Shor}}^{(\text{Non-Typed})} = 79\%$ for $\sigma = 0.01$ and $L = 4$ to leading order in L in the exponent of F_{adder} , in excellent agreement with Fig. 1. An equivalent computation for the symmetric case based on (9), together with a proper normalization of (7), i.e., $\sum_{l < 2^{L-1}} |R|^2 = 1$, results in 89%, which is in satisfactory agreement with the simulation results shown in Fig. 1.

We also note in passing that we observe an extra boost of fidelity when we introduce more qubits to the quantum circuit than necessary (see Fig. 5). We find the smallest subcircuit that exhibits such an extra boost to be the modulo addition gate, whose fidelity as a function

of the number of extra qubits ΔL appears in Figs. 5 c and d. In fact, in Fig. 3, different color symbols represent different numbers of extra qubits used in the modulo-addition gate, clearly indicating the presence of this extra boost.

A crude, simple analytical analysis may be performed on the modulo-addition gate based on our previous results, in order to show this extra boost exhibited in Figs. 5 c and d. To a very crude approximation, the limiting distribution $|R(x)|^2$ in (7), in the limit of small σ , may be approximated as a delta-peak centered at the ideal output x_0 with a uniform distribution throughout the rest of the domain of the integral in (8), such that $\int_0^1 |R(x)|^2 dx = 1$. Now, R in (5) shows that increasing L while keeping addends the same does not change R for an ideal output. Thus, together with $|R|^2 \approx F_{\text{adder}}\delta(x - x_0) + (1 - F_{\text{adder}})$ for $x \in [0, 1)$, we obtain $P_{\text{remain}} \approx F_{\text{adder}} + (1 - F_{\text{adder}})[0.5 + \sin(\pi x_0)/\pi]$, where $x_0 = N/2^{L_{\text{min}} + \Delta L}$. Despite its crudeness, the fidelity of the corresponding circuit $F_{\text{s.s.}} = P_{\text{remain}}^2$ shows a clear extra-boost behavior as a function of ΔL , demonstrating the power of our analytical model.

Discussion

Clearly, our analytical results scale in the number of qubits, demonstrating that the symmetry-driven fidelity boost will persist as we scale up the quantum circuit. We also notice that the analytically predicted fidelity [see e.g. (6) and (9)] underestimates the numerically observed fidelity boost. This is so, because our analytical analyses are based on local estimates of fidelity boosts that are focused on individual building blocks, such as adders and modulo adders. Thus, since the boosts in the individual building blocks are undeniably present, we take the boosts obtained on the basis of the individual building blocks as a lower limit of the globally achievable boost, which, as we demonstrated explicitly with our Shor algorithm simulations, may be as large as a factor 10. We expect additional boosts due to long-range coherences that are not currently contained in our local analytical estimates. These need to be investigated further in order to identify their origins and working principles.

We are certain that our results are a welcome boon for quantum experimentalists and engineers. Not only is the quantum computer already resilient against irremovable hardware errors, but, as we showed in this paper, exhibits significant performance enhancement just by controlling the symmetry of the errors. We also showed that using symmetry as a method

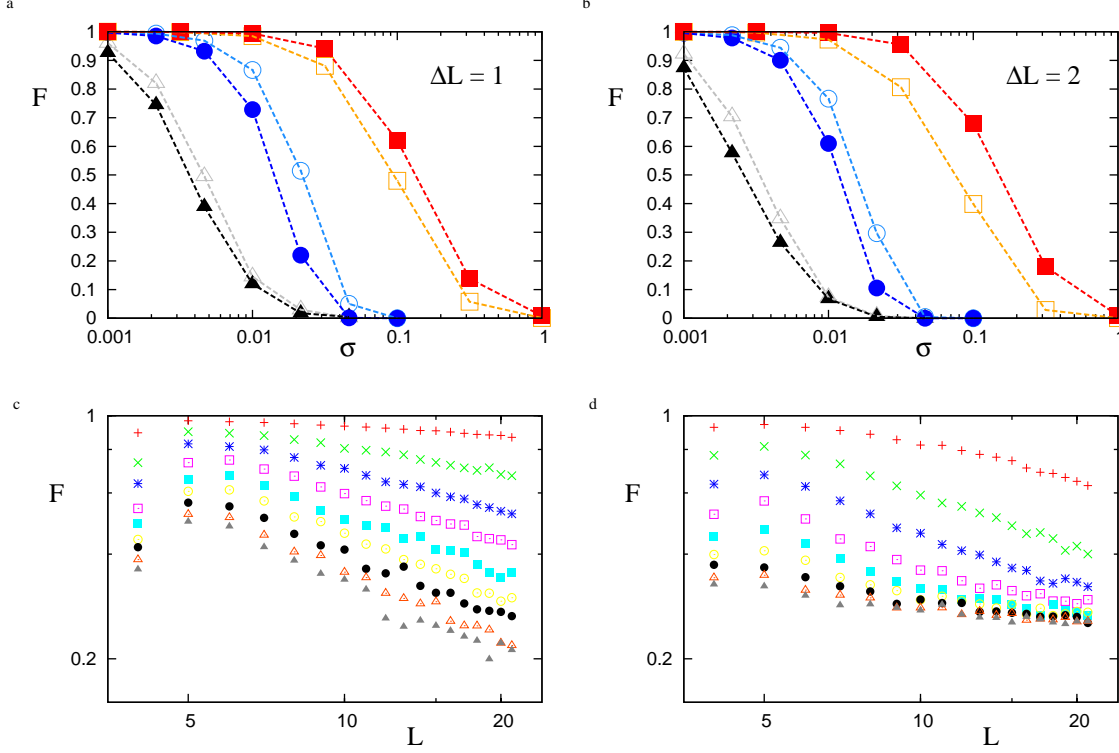


FIG. 5: Fidelity F of quantum computers running Shor's algorithm (a and b), and a modulo addition gate (c and d). In the order of a and b, the quantum computer is equipped with adders that are capable of being used in Shor-algorithm factoring of 5- and 6-bit semiprimes. Compared to Fig. 1, the boost from symmetrized errors is more significant when factoring 15, as shown. Frames c and d show F as a function of the bit-length L of the maximal semiprime that may be factored using a modulo-addition gate, equipped with relative and absolute symmetric errors, respectively. All cases were performed with $N = 15$. In decreasing order of F , different plot symbols refer to $\sigma = 0.1, 0.2, \dots, 0.9$.

to boost performance is well within engineering capabilities. This is supported by the fact that spin-echoes [29], e.g., already proved useful for practical applications in suppressing the naturally occurring errors in a given physical system. While it is still true that the symmetry needs to be implemented to a high precision, from the engineering perspective, the task of keeping the symmetry should be easier than keeping the error level itself small. Our results are also of interest to theorists. Given that exploiting symmetry is the key for the dramatic fidelity boost at the architectural, surface level, as opposed to the individual,

microscopic, inner-workings of a single-qubit state, we gain the insight that a topologically and structurally robust quantum algorithm may be developed. Given the fact that quantum algorithms, in general, tend to contain a large number of symmetric structures, we expect that designing hardware that results in symmetric errors, as exploited in this paper, may be beneficial for boosting performance in other quantum algorithms as well.

It would have been lamentable if the irremovable hardware errors in the logical qubits proliferated too quickly for a quantum computer to be of practical use. Fortunately, as we showed in this paper, this is not so. Together with the pioneering works in quantum error correction and its fault-tolerant implementation, the surprising robustness of quantum computers with respect to errors and noise suggests that quantum computing and quantum information are more than just of academic interest. Exploiting symmetry in the subunits of quantum algorithms as suggested in this paper provides an additional powerful tool on the way to the construction of quantum computers of practical importance.

ADDITIONAL INFORMATION

Competing financial interests: The authors declare no competing financial interests.

-
- [1] Nielsen, M. A. & Chuang, I. L. *Quantum Computation and Quantum Information* (Cambridge Univ. Press, 2000).
 - [2] Shor, P. W. *Proc. 35th Annual Symp. Foundations of Computer Science* 124-134 (IEEE, 1994).
 - [3] Rivest, R., Shamir, A., & Adleman, A. A method for obtaining digital signatures and public-key cryptosystems. *Comm. ACM* **21** (2), 120-126 (1978).
 - [4] Landauer, R. *Quantum Computing and Communications*, edited by M. Brooks (Springer, 1999), 61.
 - [5] Shor, P. W. Scheme for reducing decoherence in quantum computer memory. *Phys. Rev. A* **52** R2493-R2496 (1995).
 - [6] Steane, A. M. Error correcting codes in quantum theory. *Phys. Rev. Lett.* **77**, 793-797 (1996).
 - [7] Calderbank, A. R. & Shor, P. W. Good quantum error-correcting codes exist. *Phys. Rev. A* **54**, 1098-1105 (1996).

- [8] Laflamme, R., Miquel, C., Paz, J. P. & Zurek, W. H. Perfect quantum error correcting code. *Phys. Rev. Lett.* **77** 198 (1996).
- [9] Shor, P. W. *Proc. 37th Annual Symp. Foundations of Computer Science* 56-65 (IEEE,1996).
- [10] Steane, A. M. Fault-tolerant quantum computing. *Nature* **399**, 124-126 (1999).
- [11] Gottesman, D. Theory of fault-tolerant quantum computation. *Phys. Rev. A* **57**, 127-137 (1998).
- [12] Fowler, A. G., Mariantoni, M., Martinis, J. M. & Cleland, A. N. Surface codes: Towards practical large-scale quantum computation. *Phys. Rev. A* **86**, 032324 (2012).
- [13] Fowler, A. G., Whiteside, A. C., McInnes, A. L. & Rabbani, A. Topological code Autotune. *Phys. Rev. X* **2**, 041003 (2012).
- [14] Barends, R. *et al.* Superconducting quantum circuits at the surface code threshold for fault tolerance. *Nature* **508**, 500-503 (2014).
- [15] Muhonen, J. T. *et al.* Storing quantum information for 30 seconds in a nanoelectronic device. *Nat. Nanotech.* **9**, 986-991 (2014).
- [16] Beauregard, S. Circuit for Shor's algorithm using $2n+3$ qubits. *Quantum Inf. and Comput.* **3**, 175-185 (2003).
- [17] Markov, I. L. & Saeedi, M. Constant-optimized quantum circuits for modular multiplication and exponentiation. *Quantum Inf. Comput.* **12**, 361-394 (2012).
- [18] Cirac, J. I. & Zoller, P. Quantum computations with cold trapped ions. *Phys. Rev. Lett.* **74**, 4091-4094 (1995).
- [19] Miquel, C., Paz, J. P. & Perazzo, R. Factoring in a dissipative quantum computer. *Phys. Rev. A* **54**, 2605-2613 (1996).
- [20] Miquel, C., Paz, J. P. & Zurek, W. H. Quantum computation with phase drift errors. *Phys. Rev. Lett.* **78**, 3971-3974 (1997).
- [21] Wei, L. F., Li, X., Hu, X. & Nori, F. Effects of dynamical phases in Shor's factoring algorithm with operational delays. *Phys. Rev. A* **71**, 022317 (2005).
- [22] García-Mata, I., Frahm, K. M. & Shepelyansky, D. L. Shor's factorization algorithm with a single control qubit and imperfections. *Phys. Rev. A* **78**, 062323 (2008).
- [23] Wecker, D. & Svore, K. M. LIQUi|>: A software design architecture and domain-specific language for quantum computing. Preprint at <http://arxiv.org/abs/1402.4467> (2014).
- [24] García, H. J. & Markov, I. L. Simulation of quantum circuits via stabilizer frames. *IEEE*

- Trans. on Comput.* **64**, 2323-2336 (2014).
- [25] Nam, Y. S. & Blümel, R. Robustness and performance scaling of a quantum computer with respect to a class of static defects. *Phys. Rev. A* **88**, 062310 (2014).
 - [26] Nam, Y. S. & Blümel, R. Robustness of the quantum Fourier transform with respect to static gate defects. *Phys. Rev. A* **89**, 042337 (2014).
 - [27] Nam, Y. S. & Blümel, R. Performance scaling of the quantum Fourier transform with defective rotation gates. *Quantum Inf. Comput.* **15**, 721-736 (2015).
 - [28] Nam, Y. S. & Blümel, R. Analytical formulas for the performance scaling of quantum processors with a large number of defective gates, *Phys. Rev. A* **92**, 042301 (2015).
 - [29] Hahn, E. L. Spin echoes. *Phys. Rev.* **80**, 580-594 (1950).

AUTHOR CONTRIBUTIONS

Y. S. Nam and R. Blümel devised the idea and wrote the main manuscript. Y. S. Nam analyzed the results.